https://doi.org/10.1016/j.cmpb.2021.106408

Biomechanical Comparison among Five Mid/hindfoot Arthrodeses Procedures in Treating Flatfoot Using a Musculoskeletal Multibody Driven Finite Element Model

Yinghu Peng [a,b], Wenxin Niu [c,d], Duo Wai-Chi Wong [a,b], Yan Wang [a,b], Tony Lin-Wei Chen [a], Guoxin Zhang [a], Qitao Tan [a], Ming Zhang [a,b*]

[a] Department of Biomedical Engineering, Faculty of Engineering, Hong Kong Polytechnic University, Hong Kong SAR, 999077, China

[b] Hong Kong Polytechnic University Shenzhen Research Institute, Shenzhen, 518057, China

[c] Shanghai Yangzhi Rehabilitation Hospital, Tongji University School of Medicine, Shanghai, 201619, China

[d] Clinical Center for Intelligent Rehabilitation Research, Tongji University, Shanghai, 201619, China

*Corresponding author: Prof. Ming Zhang

1 Department of Biomedical Engineering, Faculty of Engineering,

2 The Hong Kong Polytechnic University,

3 Hung Hom, KLN,

4 Hong Kong, China

5 Email: ming.zhang@polyu.edu.hk

Abstract

Background and Objective

Mid/hindfoot arthrodesis could modify the misalignment of adult-acquired flatfoot and attenuate pain. However, the long-term biomechanical effects of these surgical procedures remain unclear, and the quantitative evidence is scarce. Therefore, we aimed to investigate and quantify the influences of five mid/hindfoot arthrodeses on the internal foot biomechanics during walking stance.

Methods

A young participant with flexible flatfoot was recruited for this study. We reconstructed a subject-specific musculoskeletal multibody driven-finite element (FE) foot model based on the foot magnetic resonance imaging. The severe flatfoot model was developed from the flexible flatfoot through the attenuation of ligaments and the unloading of the posterior tibial muscle. The five mid/hindfoot arthrodeses simulations (subtalar, talonavicular, calcaneocuboid, double, and triple arthrodeses) and a control condition (no arthrodesis) were performed simultaneously in the detailed foot multibody dynamics model and FE model. Muscle forces calculated by a detailed multi-segment foot model and ground reaction force were used to drive the foot FE model. The internal foot loadings were compared among control and these arthrodeses conditions at the first and second vertical ground reaction force (VGRF) peak and VGRF valley instants.

Results

The results indicated that the navicular heights in double and triple arthrodeses were

higher than other surgical procedures, while the subtalar arthrodesis had the smallest values. Five mid/hindfoot arthrodeses reduced the peak plantar fascia stress compared to control. However, double and triple arthrodeses increased the peak medial cuneo-navicular joint contact pressures and peak foot pressures as well as the metatarsal bones stresses.

Conclusion

Although mid/hindfoot arthrodesis generally reduced the collapse of medial longitudinal arch and plantar fascia loading during the stance phase, the increased loading in the adjacent unfused joint and metatarsal bones for double and triple arthrodeses should be noted. These findings could account for some symptoms experienced by flatfoot patients after surgery, which may facilitate the optimization of surgical protocols.

Keyword: Foot-ankle complex; Flatfoot; Mid/hindfoot arthrodesis; Musculoskeletal multibody model; Finite element analysis

1. Introduction

Adult-acquired flatfoot (AAF) is a progressive foot disease characterized by the collapse of the medial longitudinal arch and deformity of the foot-and-ankle complex. The prevalence of flatfoot among the adult population could be as high as 23% [1, 2]. Existing studies revealed some risk factors for AAF, including obesity, foot injury, and fatigue, while posterior tibial tendon dysfunction (PTTD) was considered the leading cause of AAF [3]. The progressed flatfoot with severe PTTD (in stages III and IV) could induce a rigid foot that leads to various symptoms, including swelling around the ankle, foot pain, and immobility. Surgical treatments are recommended to attenuate pain and restore normal foot arch for patients with end-stage AAF [4].

Mid/hindfoot arthrodeses are surgical options to treat end-stage flatfoot. The arthrodeses, including subtalar, talonavicular, calcaneocuboid, double (talonavicular and calcaneocuboid), and triple (subtalar, talonavicular, and calcaneocuboid), are widely used to help patients correct foot alignment, relieve pain and restore function [5-10]. Though clinically effective, these salvage procedures inevitably affect the mobility of the mid/hindfoot and could contribute to the degenerative changes of unfused joints [5, 7, 11]. A previous study reported that talonavicular arthrodesis was associated with an increased risk of adjacent joint deformities and progressive osteoarthritis [7]. Isolated calcaneocuboid joint arthrodesis also caused degenerative arthritis in the surrounding joints [11]. Additionally, some patients with triple arthrodesis developed osteoarthritis around the midfoot joint [5]. The complications could be associated with the alteration of internal foot loading and transfer due to joint

fusion; thus, evaluating the biomechanical effects of these procedures should be noted.

To evaluate the biomechanical effects of mid/hindfoot arthrodesis, various analysis approaches have been adopted. Some studies have adopted cadaveric experiments to assess the foot arch and joint interface pressure [6, 12], which could implicate potential complications and functional outcomes of surgical treatments. Gait analysis and fluoroscopic imaging system were also used to evaluate the kinematic outcomes of the mid/hindfoot arthrodesis on patients with flatfoot during walking [13-15]. However, more detailed internal biomechanical information, such as stress distributions of the bones and soft tissues, is not easy to measure by experimental approaches.

Finite element (FE) analysis provides an alternative to evaluating internal stress and strain, which could provide direct investigations on the pathomechanics of the musculoskeletal system [16-20]. Previous FE foot models have investigated the functional outcomes of surgical treatments on flatfoot [17-19, 21, 22]. One study targeted midfoot arthrodesis in treating severe flatfoot and suggested that naviculocuneiform arthrodesis increased the stress of the spring ligament [22]. Another study also evaluated the stress of the soft tissue under isolated, double and triple mid/hindfoot arthrodeses [18]. However, these simulation studies were confined to static conditions [17, 22, 23]. Although some studies used the foot muscle forces and ground reaction forces to drive the foot FE model, the muscle forces were normally estimated from electromyography (EMG) data in previous literature, which could not provide subject-specific boundary conditions for the FE model [18, 19]. The effects of mid/hindfoot arthrodesis on the internal foot dynamics in patients with flatfoot during

walking warrant further investigation.

This study aims to develop a subject-specific musculoskeletal multibody (MSK) driven-FE foot model to investigate the effects of mid/hindfoot arthrodesis on internal foot biomechanics. Five mid/hindfoot arthrodeses were simulated in the detailed multi-segment foot model and FE model simultaneously. The foot muscle forces calculated by the detailed multi-segment foot model [24] and ground reaction forces were used as the inputs for the FE models. The predicated internal foot biomechanics of walking stance among five mid/hindfoot surgical approaches in the foot-ankle complex model were compared.

2. Materials and Methods

A young male adult of age 28, height 175 cm and mass 62.5 kg with flexible flatfoot was involved. The footprint index [25] and the navicular drop test [26] were used to determine the foot type. The participant's right foot was classified as flatfoot, with a high arch index (>0.26) and a large navicular drop (> 10 mm) [25, 26]. Except for the flatfoot, the participant did not have any neuromuscular diseases or biomechanical abnormalities. We developed an MSK-driven flatfoot FE model with 3D plantar fascia geometry based on foot magnetic resonance imaging (MRI), which could evaluate the effects of mid/hindfoot arthrodesis in the internal foot biomechanics (Figure 1). The modeling procedures, including data collection, geometries reconstruction, materials properties, mid/hindfoot arthrodesis configurations, boundary conditions, and model validation, were described.

2.1 Experimental protocol

A gait analysis system, including eight cameras (Vicon, Oxford Metrics Ltd., Oxford, England) and four force plates (OR6, AMTI, Watertown, United States) was used. The Vicon cameras and force plate data were collected synchronously with sampling frequencies at 100 Hz and 1000 Hz. Reflective markers were placed on the surface of the foot and leg according to the protocol in the previous study [27]. Detailed foot marker placements could be seen in Figure 2(a). The marker trajectories and ground reaction force of the static trial and walking trials were collected. During the data collection process, the patient was asked to walk at a comfortable speed and avoid staring at the equipment. The dynamic foot plantar pressure was also collected using the pressure measurement system F-scan (Tekscan Inc., Boston, USA), seen in Figure 2(b). Additionally, the electromyography device (Delsys Inc., Boston, MA) was used to record surface electromyography (EMG) signals, including the gastrocnemius medialis (GM), gastrocnemius lateralis (GL), soleus (SL), tibialis anterior (TA), and peroneus longus (PL). To accurately scale the detailed foot MSK model, the geometry of the right foot was also collected using a 3D foot surface scanner (UPOD-HDS; ScanPod3D, Wuhan, China). The geometry of the right foot can be seen in Figure 2(c).

2.2 Musculoskeletal multibody foot model

The joint and foot muscle forces were estimated using the Glasgow-Maastricht foot model in the Anybody Modeling software (AnyBody Technology, Aalborg, Denmark, version 6.0.5) [24, 28]. In this model, an advanced multi-segment foot MSK model was adopted, which encompassed the detailed foot bones, foot muscles, and ligaments [24]. The force plate data and reflective marker trajectories obtained from

the motion capture system were used as inputs for the MSK model. The computational process of the model could be divided into three parts, static optimization, inverse kinematic, and inverse dynamics [29]. In the first step, collected static data were used to scale the bone geometry and determine the locations of the virtual markers in the model. To accurately scale the foot bone geometries of the model, scanned foot geometry was used to register the original foot geometry with the radial basis function [30]. After static optimization, the walking trial data were used to calculate the joint kinematics parameters through inverse kinematic analysis. In the inverse dynamics, the muscle forces and joint mechanics could be predicted. The predicted muscle forces were validated by comparing the model-simulated muscle activation with the surface EMG [31]. The workflow of MSK model calculation is demonstrated in Figure 3.

2.3 Finite element model

2.3.1 Model Reconstruction

The MRI data of the right foot were obtained in a neutral, non-weight-bearing condition with the 3.0-T MRI scanner (Seimens, Erlangen, Germany). The foot-ankle complex geometries, including the encapsulated bulk tissue and bones, were segmented using medical image processing software (Mimics 10.1, Materialize Inc., Belgium). The skin layer was modeled by a 2-mm thickness membrane covering the bulk soft tissue. The three-dimensional plantar fascia was constructed. The second to fifth interphalangeal joints are fused to simplify the model. Additionally, 110 trusses were built to represent the ligaments connecting the bony structures. The plantar fascia was inserted to the inner bulk soft tissue, calcaneal tuberosity, and proximal phalanx. The

interior surface of the encapsulated soft tissue was tied to the bony structures. The foot muscles were modeled as connectors in the model. A frictionless contact algorithm with a non-linear contact stiffness was assigned to the bone contact pairs to resemble the cartilage function [32], while the geometry of the cartilage was not constructed. A friction coefficient of 0.6 was assigned to contact property between the foot surface and ground plate [33]. Figure 4 illustrates the detailed geometry of the foot FE model components.

The meshes of the foot-ankle complex components were created in Abaqus 6.14 (Simulia, Dassault Systemes, France). The material and mesh properties of the model are presented in Table 1. Mesh convergence test was conducted in complete foot model under three gait instants with a reduction of element size of 10%. The deviations of the peak plantar pressure were 2.3 - 3.8%, respectively. The mesh size in the current simulation was regarded as acceptable with assumed criteria of less than 5% deviation [34].

2.3.2 Boundary and loading conditions

The internal foot biomechanics were investigated at three stance instants, including the first peak of the vertical ground reaction force (VGRF), VGRF valley, and the second peak VGRF (Figure 5). The proximal cross-sectional surfaces of the tibia and fibula were fixed at all degrees of freedom. The ground reaction forces in three directions were applied beneath the rigid plate. The relative orientation between ground and foot was assigned based on the gait analysis data at the three gait instants by rotating the ground plate. The calculated muscle forces, including the TA, tibialis posterior,

peroneus brevis, PL, Achilles tendon (gastrocnemius and soleus), flexor hallucis longus, and flexor digitorum longus, were applied to the foot FE model through the muscle connectors. More information about the loading and boundary conditions is included in Supplementary File 1.

2.3.3 Realization of mid/hindfoot arthrodesis procedure in the model

We constructed the end-stage flatfoot simulation model by removing the tibialis posterior muscle in the MSK-driven flatfoot model since the PTTD is one of the most common causes of the end-stage AAF. Meanwhile, the strength of the spring ligament, the short plantar ligament, and the portions of the long plantar ligament, and the plantar aponeurosis were reduced by 50% to simulate the stretching of these supporting structures [35].

Mid/hindfoot arthrodesis procedures, including subtalar, talonavicular, calcaneocuboid, double, and triple arthrodeses, and control (no arthrodesis), were simulated both in the multi-segment foot MSK model and foot FE model. In the detailed musculoskeletal foot model [24], the degrees of freedom of the corresponding joints were locked to simulate the mid/hindfoot arthrodesis. Foot muscle forces were calculated as the boundary conditions for the FE model with mid/hindfoot arthrodesis. A "tie" property was defined to fuse the bones in the FE foot model. The demonstration of the mid/hindfoot arthrodesis procedures is presented in Figure 6.

2.3.4 Model output and analysis

The simulation was conducted using the standard static solver. The foot contact pressure, von Mises stress of the plantar fascia, navicular height, midfoot joint contact

pressures, and von Mises stresses of the metatarsal shaft were reported and compared among five mid/hindfoot arthrodeses and control conditions. Navicular height was measured as the distance between the navicular tuberosity and the ground surface. The peak contact pressure at three midfoot joints, including lateral cuneo-navicular (LCN), intermediate cuneo-navicular (ICN), medial cuneo-navicular (MCN) were reported.

3. Results

3.1 Validation

The plantar pressure distributions of the barefoot walking among the FE model predictions and measurements were compared. The foot pressure distribution was divided into eight masks: the medial heel, lateral heel, medial midfoot, lateral midfoot, first metatarsal, second and third metatarsal, fourth and fifth metatarsals, and hallux (Figure 7). The maximum contact pressure in each region was extracted for analysis unless the maximum value is zero. The Pearson correlation analysis [36] was performed to evaluate the agreement between measurements and predictions using 17 data pairs. The correlation analysis between the model prediction and measurement is shown in Figure 8. The correlation analysis showed that the measurement and prediction were significantly associated ($r = 0.95$, $p < 0.001$). Based on the validation results, our model prediction was considered reasonable.

3.2 Navicular height

The navicular heights among the mid/hindfoot arthrodesis simulations and control are shown in Figure 9. The navicular heights in the five mid/hindfoot arthrodeses increased at three gait instants compared to control. In the VGRF valley, the navicular

heights in five arthrodeses were almost the same. In the first and second VGRF peak, triple arthrodesis had higher navicular heights (30.8 mm and 33.2 mm) than other surgical procedures. Additionally, subtalar arthrodesis had the lowest navicular heights (29.1 mm in the first VGRF peak and 31.3 mm in the second VGRF peak) among the five arthrodeses simulations.

3.3 Plantar contact pressures

The predicted foot contact pressure distributions for mid/hindfoot arthrodesis simulations and control are shown in Figure 10. The control condition had higher peak contact pressures (0.132 MPa in the first VGRF peak and 0.138 MPa in the second VGRF valley) in the midfoot region than those of five mid/hindfoot arthrodeses simulations; however, lower peak foot contact pressure at three gait instants. Among these surgical treatments, triple arthrodesis had the highest peak foot pressures in the VGRF valley (0.251 MPa) and second VGRF peak (0.721 MPa), respectively. Further details are shown in Figure 10.

3.4 Plantar fascia stress distribution

The von Mises stress of plantar fascia for mid/hindfoot arthrodesis simulations and control are shown in Figure 11. The regions tied to the foot bones were excluded from the contour. The remaining part of the fascia was divided equally into three parts. Compared to the control condition, five surgical treatments reduced the peak plantar stress by 10 – 60%. Triple arthrodesis was more effective in reducing the plantar fascia stress (24% in the first VGRF peak, 60% in VGRF valley, and 47% in the second VGRF peak) than the other arthrodeses. However, subtalar arthrodesis had the highest peak

plantar fascia stress at the first VGRF peak (8.8 MPa) and VGRF valley (7.9 MPa) among the five arthrodeses.

3.5 Joint contact pressure

The peak midfoot joint contact pressures among five mid/hindfoot arthrodeses and control conditions are compared in Figure 12. For the peak contact pressure of MCN, double and triple arthrodeses increased the peak contact pressures by 18 – 30% at three gait instants compared to the control condition. The other three arthrodeses had little influence on the MCN, except that subtalar arthrodesis increased the peak values in the first VGRF peak. For the contact pressures of ICN, mid/hindfoot arthrodesis, except for the calcaneocuboid arthrodesis, increased the peak values in the second VGRF peak and VGRF valley. However, the peak contact pressures of the LCU in the five mid/hindfoot arthrodeses were overall reduced (17 – 28 % in the first VGRF peak, 13 -33 % in VGRF valley, and 11 - 56% in the second VGRF peak).

3.6 Stress of the metatarsal shaft

The stress distribution patterns of the metatarsal shaft under five mid/hindfoot arthrodeses and control conditions are shown in Figure 13. In the first VGRF peak, talonavicular had the highest peak values for the second (17.5 MPa) and third metatarsal shaft (10 MPa). Double and triple arthrodeses had higher peak values for the second metatarsal shaft but lower values for the third metatarsal shaft compared to the control condition. All arthrodeses had lower peak values for the second (10 – 12 MPa) and third metatarsal (12 – 18 MPa) shaft in the VGRF valley but higher peak values in the second VGRF peak compared to control condition. Further details are presented in Figure 14.

4. Discussion

This study proposed an MSK-driven flatfoot FE model, which could be used to investigate the loading distribution on the soft tissue. The detailed multi-segment foot MSK modeling [24] was first used to drive the foot FE model with surgical simulation. Compared to previous studies [17, 19], the proposed model could provide a subject-specific boundary condition of the stance phase for the FE model. The biomechanical outcomes of five mid/hindfoot arthrodeses during walking condition on internal foot loading were simultaneously investigated and could provide an informative evaluation of five treatment options.

Surgical treatments, such as mid/hindfoot arthrodesis, can modify the foot posture, especially in maintaining the medial foot arch. Previous clinical studies also indicated that arthrodesis could correct the collapsed foot arch [6, 9, 11]. This study showed that navicular heights in five surgical simulations were higher than control condition at three gait events. The results also indicated that calcaneocuboid arthrodesis and subtalar arthrodesis were less effective in maintaining the medial foot arch, especially in the first VGRF peak and the second VGRF peak. Talonavicular arthrodesis achieved a similar result with the double arthrodesis in maintaining the medial longitudinal arch at the three gait events, which further confirmed the substitution of talonavicular arthrodesis for double arthrodesis [37]. Triple arthrodesis obtained higher arch height than other surgical treatments during the walking condition. One previous cadaveric study has also investigated five mid/hindfoot arthrodeses in static condition and indicated similar results [6]. The triple arthrodesis was a more restrictive treatment for

AAF, providing a more stable foot arch for the patients.

Adults with flatfoot were typically accompanied by the collapse of the longitudinal foot arch and high foot contact area than the normal foot [38]. Mid/hindfoot arthrodesis could modify the pronation of the hindfoot and prevent the excessive collapse of the longitudinal foot arch, thus reducing the midfoot pressures [6]. The results indicated that the peak midfoot pressures in five mid/hindfoot arthrodeses were lower than those in the control group during the first VGRF peak and VGRF valley, indicating a stable foot arch. Compared to the other three arthrodeses treatments, double and triple arthrodeses achieved lower peak midfoot pressures, in line with the previous cadaver study [6]. However, these arthrodesis procedures demonstrated higher peak hindfoot and forefoot pressures at the first and second VGRF peak, respectively. The increased peak forefoot pressures should be noted, as increased peak pressures in the forefoot could potentially contribute to metatarsalgia [39].

Although the mid/hindfoot arthrodesis corrected the misalignment of the AAF, these surgical treatments could inevitably constraint the motion of the hindfoot, thus affecting the loading distribution of the adjacent joints, bone, and soft tissues [17, 19]. A previous study has reported that excessive hindfoot pronation in flatfoot caused increased foot length and increased loading on the plantar fascia, thus contributing to plantar foot pain [40]. This study indicated that all mid/hindfoot arthrodeses reduced the peak plantar fascia stress at the three gait events. The triple arthrodesis obtained the best decrease rates at three gait events (stress reduction of 24 – 67 %), which matched the previous study [17]. Additionally, the decrease rates for talonavicular (18 – 44 %),

calcaneocuboid (12 – 41 %), double arthrodesis (10 – 44 %) were similar. However, subtalar arthrodesis reduced the plantar fascia stress by 6 – 16 % compared to the control condition. These results indicated that subtalar arthrodesis is the least effective for correcting the plantar arch structure in the control condition, which was in line with previous computational studies [17, 19].

The loss of mid/hindfoot mobility was the most common side-effect of the mid/hindfoot, which might affect the load transfer from the hindfoot to the forefoot and load distribution of metatarsal bones [20]. The double and triple arthrodeses had higher peak MCN contact pressures when compared to other treatments at three gait events. Additionally, the triple arthrodesis had the highest peak ICN contact pressure during the second VGRF peak. The higher joint contact pressures could increase the rates of midfoot joint osteoarthritis, which was in line with the previous long-term clinical study of triple arthrodesis [5]. Meanwhile, other mid/hindfoot arthrodeses increased the peak joint contact pressures of the unfused joint when compared to control. The higher joint contact pressures could also account for the consecutive arthritis of the midfoot joints [18]. Additionally, mid/hindfoot could further increase the loading in the metatarsal bones. The results indicated that the second and third metatarsal bones sustained much higher stress than the other metatarsal bones in the second VGRF peak. It was reported that patients with foot and ankle surgery suffered from the fracture of the second metatarsal, which resulted from high von Mises stress [20]. Triple arthrodesis had higher stress increases in these two bones compared to the other arthrodeses in the second VGRF peak. As the von Mises stress is considered to be the predictor for the

bony stress fracture [41], it can be speculated that patients with triple arthrodesis are more susceptible to stress fractures in the second or third metatarsal bones.

Previous surgical treatment simulations typically adopted static conditions or simplified muscle loading estimated by EMG [17, 19], which were difficult to provide subject-specific boundary conditions for the foot FE model. This study has adopted the MSK-driven FE foot model, which could improve the prediction accuracy and enhance the reliability of the simulation [42]. Additionally, although several surgical treatments adopted the muscle-driven foot FE model, these surgical procedures were only performed in the foot FE models [18-20]. Our study has performed mid/hindfoot foot arthrodesis simulations in both the foot FE and foot MSK models. These procedures were almost impossible to be performed in one or two segment foot MSK models, which were widely used in previous muscle-driven foot FE models [31, 42]. The foot muscle forces obtained from the detailed multi-segment foot MSK model [24] with surgical treatment could provide consistent boundary conditions for the foot FE model.

This study assumed an end-stage flatfoot model using a mild case with attenuated soft tissue properties because the end-stage flatfoot compounded with other foot deformities with different severities, such as hindfoot valgus and hallux valgus that made it difficult to justify a representative case. Some literature proposed the use of a surrogate by attenuating ligaments and unloading the posterior tibial muscles on the normal foot model [19, 35]. We believed that this approach could still partially resemble some level of medial arch collapse, hindfoot valgus and degeneration of soft tissue in case of the end-stage flatfoot. Though FE is confined to nonclinical theoretical research

tool to supplement surgical decisions, researchers shall aware on the limits of model applications due to model assumption [43]. Nonetheless, the strength of this study was the endeavour to drive the foot model using a model subject specific MSK model that improved the credibility in the boundary and loading conditions.

In this study, several limitations should be noted. First, the material properties used for the bony structures and soft tissues were obtained from previous literature, which could underestimate the prediction accuracy of the model. Second, the subject-specific approach for the foot-ankle complex FE analysis was employed in this study, which could hinder the generalizability of the findings. However, due to the limitation of the complex foot structures and boundary conditions in the foot-ankle complex model, single-subject models have often been used to evaluate foot biomechanics [43, 44]. This study endeavored to adopt a representative model subject of the population to account for the generalizability. Further study could be performed to consider a case series with sample size for flatfoot patients before and after surgery and acquire their boundary conditions. Third, the foot muscles in the modeling were simplified as one-dimensional, which could not account for spatial fiber orientation and interactions between muscles and bones [45]. Forth, the static MRI of the foot-ankle complex was adopted to build the FE model and replicate the foot-ground contact conditions during three walking events. However, the foot model obtained from the static foot MRI may not fully reflect the actual dynamic foot characteristics. Therefore, it is necessary to collect the dynamic foot MRI data in future work.

5. Conclusion

In this study, a subject-specific MSK driven-FE foot model was developed to investigate the effects of five mid/hindfoot arthrodeses on internal foot biomechanics of AAF. This study enabled the mid/hindfoot arthrodesis simulation in the detailed multi-segment foot model [24], thus providing the subject-specific boundary conditions (foot muscle forces) for the foot FE model with mid/hindfoot arthrodesis. The model prediction indicated that all procedures facilitated a stable foot arch and reduced plantar fascia loading during walking stance. However, double and triple arthrodeses provided comparatively better arch height at the cost of higher loading for the MCN joint and second and third metatarsal bones. The proposed model could contribute to the biomechanical understanding of mid/hindfoot surgical treatments in subject-specific flatfoot deformity interventions.

Ethics statement

The experimental protocol was approved by the Human Subjects Ethics Sub-Committee of the Hong Kong Polytechnic University (Number: HSEARS20190124008). The participant was informed of the procedures for data collection and research contents and signed the consent form.

Funding

The work was supported by the National Natural Science Foundation of China [grant number 11732015, 11972315], General Research Fund granted by the Hong Kong Research Grant Council [grant number PolyU152065/17E].

Declaration of competing interest

The authors declare that they have no conflict of interest.

REFERENCES

[1] N. Shibuya, D.C. Jupiter, L.J. Ciliberti, V. VanBuren, J. La Fontaine, Characteristics of adult flatfoot in the United States, J Foot Ankle Surg, 49 (2010) 363-368. https:// doi.org/10.1053/j.jfas.2010.04.001.

[2] Y.M. Golightly, M.T. Hannan, A.B. Dufour, J.M. Jordan, Racial differences in foot disorders and foot type, Arthritis Care Res, 64 (2012) 1756-1759. https:// doi.org/10.1002/acr.21752.

[3] R. Douglas, Biomechanics and orthotic treatment of the adult acquired flatfoot, Clin Podiatr Med Surg, 37 (2020) 71-89. https://doi.org/10.1016/j.cpm.2019.08.007.

[4] M.M. Abousayed, J.P. Tartaglione, A.J. Rosenbaum, J.A. Dipreta, Classifications in brief: johnson and strom classification of adult-acquired flatfoot deformity, Clin Orthop Relat Res, 474 (2016) 588-593. https:// doi.org/10.1007/s11999-015-4581-6.

[5] I.B. de Groot, M. Reijman, H.A. Luning, J.A. Verhaar, Long-term results after a triple arthrodesis of the hindfoot: function and satisfaction in 36 patients, Int Orthop, 32 (2008) 237-241. https:// doi.org/ 10.1007/s00264-006-0295-4.

[6] Y. Chen, K. Zhang, M. Qiang, Y. Hao, Maintenance of longitudinal foot arch after different mid/hind-foot arthrodesis procedures in a cadaveric model, Clin Biomech, 29 (2014) 170-176. https://doi: 10.1016/j.clinbiomech.2013.11.016.

[7] G.M. Weinraub, M.A. Heilala, Isolated talonavicular arthrodesis for adult onset flatfoot deformity/posterior tibial tendon dysfunction, Clin Podiatr Med Surg, 24 (2007) 745-752. https:// doi.org/ 10.1016/j.cpm.2007.06.004.

[8] B. Hintermann, J.T. Deland, C. de Cesar Netto, S.J. Ellis, J.E. Johnson, M.S. Myerson, B.J. Sangeorzan, D.B. Thordarson, L.C. Schon, Consensus on indications for isolated subtalar joint fusion and naviculocuneiform fusions for progressive collapsing foot deformity, Foot Ankle Int, 41 (2020) 1295-1298. https://doi.org/10.1177/1071100720950738.

[9] A. Bernasconi, F. Lintz, F. Sadile, The role of arthroereisis of the subtalar joint for flatfoot in children and adults, EFORT Open Rev., 2 (2017) 438-446. https:// doi.org/10.1302/2058-5241.2.170009.

[10] M.T. Burrus, B.C. Werner, J.B. Carr, V. Perumal, J.S. Park, Increased failure rate of modified double arthrodesis compared with triple arthrodesis for rigid pes planovalgus, J Foot Ankle Surg, 55 (2016) 1169-1174. https:// doi.org/10.1053/j.jfas.2016.07.001.

[11] M. Barmada, H.S. Shapiro, S.F. Boc, Calcaneocuboid arthrodesis, Clin Podiatr Med Surg, 29 (2012) 77-89. https://doi.org/10.1016/j.cpm.2011.11.002.

[12] N. Martinelli, A. Marinozzi, M. Schulze, V. Denaro, J. Evers, A. Bianchi, D. Rosenbaum, Effect of subtalar arthroereisis on the tibiotalar contact characteristics in a cadaveric flatfoot model, J Biomech, 45 (2012) 1745-1748. https:// doi.org/10.1016/j.jbiomech.2011.11.009.

[13] D.E. Westberry, J.R. Davids, J.P. Anderson, L.I. Pugh, R.B. Davis, J.W. Hardin, The operative correction of symptomatic flat foot deformities in children, Bone Joint J, 95-B (2013) 706-713. https://doi.org/10.1302/0301-620X.95B5.30594.

[14] D.V. Flores, C. Mejia Gomez, M. Fernandez Hernando, M.A. Davis, M.N. Pathria, Adult flatfoot deformity: anatomy, biomechanics, staging, and imaging findings, Radiographics, 39 (2019) 1437-1460. https://doi.org/10.1148/rg.2019190046.

[15] S. Tejero, A. Carranza-Pérez-Tinao, M.D. Zambrano-Jiménez, E. Prada-Chamorro, J.J. Fernández-Torres, A. Carranza-Bencano, Minimally invasive technique for stage III adult-acquired flatfoot deformity: a mid- to long-term retrospective study, Int. Orthop., 45 (2021) 217-223. https://doi.org/10.1007/s00264-020-04724-5.

[16] D. Wai-Chi Wong, Y. Wang, M. Zhang, A. Kam-Lun Leung, Functional restoration and risk of non-union of the first metatarsocuneiform arthrodesis for hallux valgus: A finite element approach, J Biomech, 48 (2015) 3142-3148. https://doi.org/10.1016/j.jbiomech.2015.07.013.
[17] C. Cifuentes-De la Portilla, R. Larrainzar-Garijo, J. Bayod, Analysis of biomechanical stresses caused by hindfoot joint arthrodesis in the treatment of adult acquired flatfoot deformity: A finite element study, Foot Ankle Surg, 26 (2020) 412-420. https://doi.org/10.1016/j.fas.2019.05.010.
[18] D.W.-C. Wong, Y. Wang, W. Niu, M. Zhang, Finite element analysis of subtalar joint arthroereisis on adult-acquired flexible flatfoot deformity using customised sinus tarsi implant, J. Orthop. Translat., 27 (2021) 139-145. https://doi.org/10.1016/j.jot.2020.02.004.
[19] D.W. Wong, Y. Wang, T.L. Chen, A.K. Leung, M. Zhang, Biomechanical consequences of subtalar joint arthroereisis in treating posterior tibial tendon dysfunction: a theoretical analysis using finite element analysis, Comput Methods Biomech Biomed Engin, 20 (2017) 1525-1532. https://doi.org/10.1080/10255842.2017.1382484.
[20] Y. Wang, Z. Li, D.W. Wong, M. Zhang, Effects of ankle arthrodesis on biomechanical performance of the entire foot, PLoS One, 10 (2015) e0134340. https://doi.org/10.1371/journal.pone.0134340.
[21] J.M. Iaquinto, J.S. Wayne, Effects of surgical correction for the treatment of adult acquired flatfoot deformity: A computational investigation, J. Orthop. Res., 29 (2011) 1047-1054. https:// doi.org/10.1002/jor.21379.
[22] C. Cifuentes-De la Portilla, C. Pasapula, R. Larrainzar-Garijo, J. Bayod, Finite element analysis of secondary effect of midfoot fusions on the spring ligament in the management of adult acquired flatfoot, Clin Biomech, 76 (2020) 105018. https://doi.org/10.1016/j.clinbiomech.2020.105018.
[23] J.M. Iaquinto, J.S. Wayne, Effects of surgical correction for the treatment of adult acquired flatfoot deformity: A computational investigation, J Orthop Res, 29 (2011) 1047-1054. https://doi.org/10.1002/jor.21379.
[24] M. Oosterwaal, S. Carbes, S. Telfer, J. Woodburn, S. Torholm, A.A. Al-Munajjed, L. van Rhijn, K. Meijer, The Glasgow-Maastricht foot model, evaluation of a 26 segment kinematic model of the foot, J Foot Ankle Res, 9 (2016) 1-10. https://doi.org/10.1186/s13047-016-0152-7.
[25] H. Roy, K. Bhattacharya, S. Deb, K. Ray, Arch index: an easier approach for arch height (a regression analysis), Al Ameen J Med Sci, 5 (2012) 137-146.
[26] M. Mueller, J. Host, B. Norton, Navicular drop as a composite measure of excessive pronation, J Am Podiatr Med Assoc, 83 (1993) 198-202. https://doi.org/10.7547/87507315-83-4-198
[27] M. Oosterwaal, S. Telfer, S. Tørholm, S. Carbes, L.W. van Rhijn, R. Macduff, K. Meijer, J. Woodburn, Generation of subject-specific, dynamic, multisegment ankle and foot models to improve orthotic design: a feasibility study, BMC Musculoskelet Disord, 12 (2011) 1-10. https://doi.org/10.1186/1471-2474-12-256.
[28] M. Damsgaard, J. Rasmussen, S.T. Christensen, E. Surma, M. de Zee, Analysis of musculoskeletal systems in the AnyBody Modeling System, Simul Model Pract Theory, 14 (2006) 1100-1111. https://doi.org/10.1016/j.simpat.2006.09.001.
[29] Y. Peng, D.W. Wong, Y. Wang, T.L. Chen, Q. Tan, Z. Chen, Z. Jin, M. Zhang, Immediate Effects of Medially Posted Insoles on Lower Limb Joint Contact Forces in Adult Acquired Flatfoot: A Pilot Study, Int J Environ Res Public Health, 17 (2020). https://doi.org/10.3390/ijerph17072226.
[30] M.D. Buhmann, Radial basis functions: theory and implementations, Cambridge university press2003.
[31] Y. Peng, D.W. Wong, T.L. Chen, Y. Wang, G. Zhang, F. Yan, M. Zhang, Influence of arch support

heights on the internal foot mechanics of flatfoot during walking: A muscle-driven finite element analysis, Comput Biol Med, 132 (2021) 104355. https://doi.org/10.1016/j.compbiomed.2021.104355.
[32] D.W.-C. Wong, Y. Wang, A.K.-L. Leung, M. Yang, M. Zhang, Finite element simulation on posterior tibial tendinopathy: Load transfer alteration and implications to the onset of pes planus, Clin. Biomech., 51 (2018) 10-16. https://doi.org/10.3390/ijerph17072226.
[33] M. Zhang, A.F. Mak, In vivo friction properties of human skin, Prosthet Orthot Int, 23 (1999) 135-141. https://doi.org/10.3109/03093649909071625.
[34] H.B. Henninger, S.P. Reese, A.E. Anderson, J.A. Weiss, Validation of computational models in biomechanics, Proc Inst Mech Eng H, 224 (2010) 801-812. https://doi.org/10.1243/09544119JEIM649.
[35] G.A. Arangio, K.L. Reinert, E.P. Salathe, A biomechanical model of the effect of subtalar arthroereisis on the adult flexible flat foot, Clin Biomech (Bristol, Avon), 19 (2004) 847-852. https://doi.org/10.1016/j.clinbiomech.2003.11.002.
[36] R. Taylor, Interpretation of the correlation coefficient: a basic review, J Diagn Med Sonogr, 6 (1990) 35-39. https://doi.org/10.1177/875647939000600106.
[37] S. Thelen, J. Rutt, M. Wild, T. Logters, J. Windolf, J. Koebke, The influence of talonavicular versus double arthrodesis on load dependent motion of the midtarsal joint, Arch Orthop Trauma Surg, 130 (2010) 47-53. https://doi.org/10.1007/s00402-009-0878-9.
[38] B. Chuckpaiwong, J.A. Nunley, N.A. Mall, R.M. Queen, The effect of foot type on in-shoe plantar pressure during walking and running, Gait & Posture, 28 (2008) 405-411. https://doi.org/10.1016/j.gaitpost.2008.01.012.
[39] E. Toullec, Adult flatfoot, Orthop Traumatol Surg Res, 101 (2015) S11-S17. https://doi.org/10.1016/j.otsr.2014.07.030.
[40] D.B. Irving, J.L. Cook, H.B. Menz, Factors associated with chronic plantar heel pain: a systematic review, J Sci Med Sport, 9 (2006) 11-22. https://doi.org/10.1016/j.jsams.2006.02.004.
[41] J.H. Keyak, S.A. Rossi, Prediction of femoral fracture load using finite element models: an examination of stress- and strain-based failure theories, J Biomech, 33 (2000) 209-214. https://doi.org/10.1016/s0021-9290(99)00152-9.
[42] M. Akrami, Z. Qian, Z. Zou, D. Howard, C.J. Nester, L. Ren, Subject-specific finite element modelling of the human foot complex during walking: sensitivity analysis of material properties, boundary and loading conditions, Biomech Model Mechan, 17 (2018) 559-576. https://doi.org/10.1007/s10237-017-0978-3.
[43] D.W.-C. Wong, T.L.-W. Chen, Y. Peng, W.-K. Lam, Y. Wang, M. Ni, W. Niu, M. Zhang, An instrument for methodological quality assessment of single-subject finite element analysis used in computational orthopaedics, Medicine in Novel Technology and Devices, 11 (2021) 100067. https://doi.org/10.1016/j.medntd.2021.100067.
[44] T.L.-W. Chen, D.W.-C. Wong, Y. Peng, M. Zhang, Prediction on the plantar fascia strain offload upon Fascia taping and Low-Dye taping during running, J Orthop Translat, 20 (2020) 113-121. https://doi.org/10.1016/j.jot.2019.06.006.
[45] J. Li, Y. Lu, S.C. Miller, Z. Jin, X. Hua, Development of a finite element musculoskeletal model with the ability to predict contractions of three-dimensional muscles, J Biomech, 94 (2019) 230-234. https://doi.org/10.1016/j.jbiomech.2019.07.042.
[46] C. Pailler-Mattei, S. Bec, H. Zahouani, In vivo measurements of the elastic mechanical properties of human skin by indentation tests, Med Eng Phys, 30 (2008) 599-606. https://doi.org/10.1016/j.medengphy.2007.06.011.

[47] D. Lemmon, T.Y. Shiang, A. Hashmi, J.S. Ulbrecht, P.R. Cavanagh, The effect of insoles in therapeutic footwear—A finite element approach, J Biomech, 30 (1997) 615-620. https://doi.org/10.1016/s0021-9290(97)00006-7.
[48] W.-P. Chen, C.-W. Ju, F.-T. Tang, Effects of total contact insoles on the plantar stress redistribution: a finite element analysis, Clin Biomech, 18 (2003) S17-S24. https://doi.org/10.1016/S0268-0033(03)00080-9.
[49] S. Siegler, J. Block, C.D. Schneck, The Mechanical Characteristics of the Collateral Ligaments of the Human Ankle Joint, Foot & ankle, 8 (1988) 234-242. https://doi.org/10.1177/107110078800800502.
[50] D.G. Wright, D.C. Rennels, A Study of the Elastic Properties of Plantar Fascia, JBJS, 46 (1964) 482-492.
.

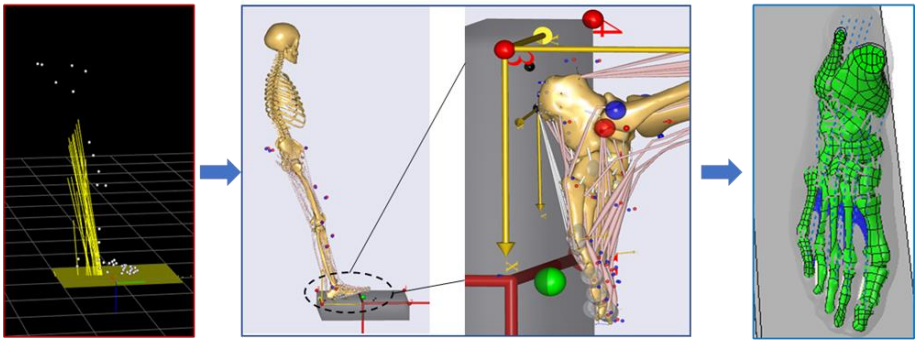

Figure 1. The workflow of the muscle-driven finite element model, including (a) gait data collection, (b) detailed foot musculoskeletal multibody model, and (c) foot finite element model

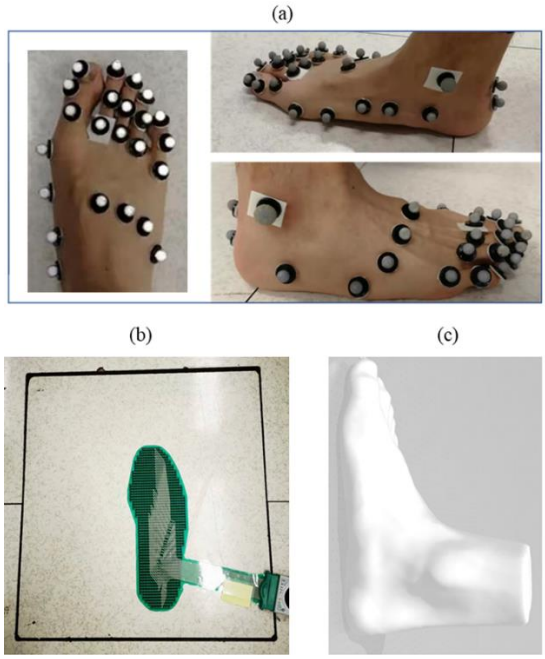

Figure 2. Experimental setup for data collection, including (a) detailed foot marker placements, (b) foot pressure sensor, and (c) foot surface geometry collection

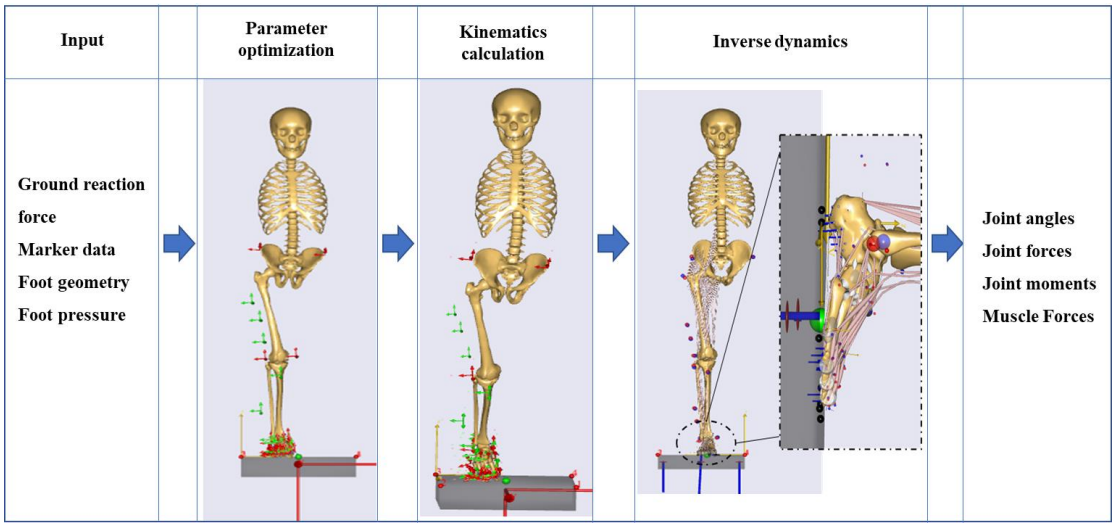

Figure 3. Workflow of the musculoskeletal multibody dynamics modeling, including parameter optimization, kinematics calculation, and inverse dynamics.

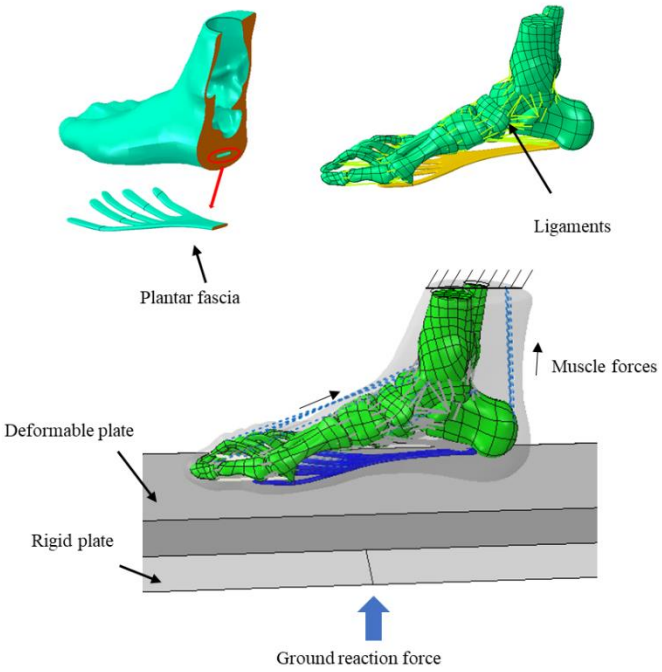

Figure 4. Geometrical configuration and boundary/loading conditions of the finite element model of the foot-and-ankle complex.

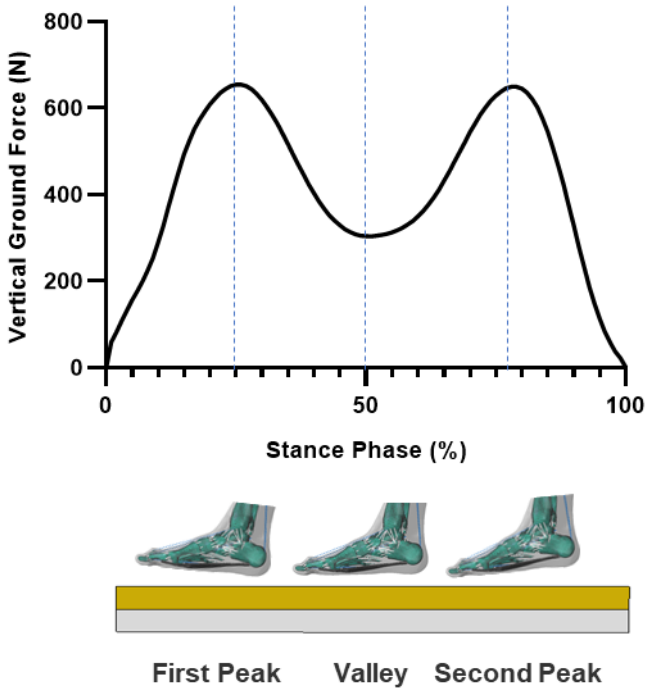

Figure 5. An illustration of the three stance instants from the vertical ground reaction forces during the stance phase

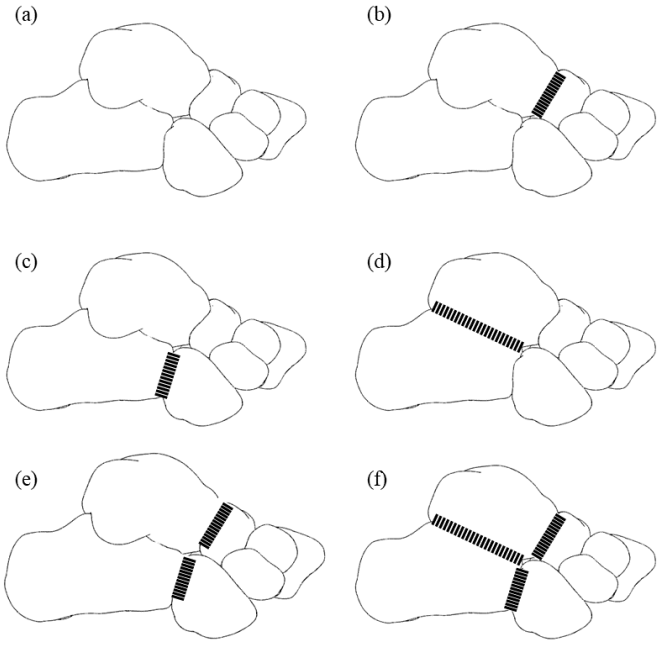

Figure 6. Surgery demonstration of control and five mid/hindfoot arthrodeses, including (a) control condition, (b) talonavicular arthrodesis, (c) calcaneocuboid arthrodesis, (d) subtalar arthrodesis, (e) double arthrodesis, and (f) triple arthrodesis. The arthrodesis was simulated by fusing the bones using the "tie" operation.

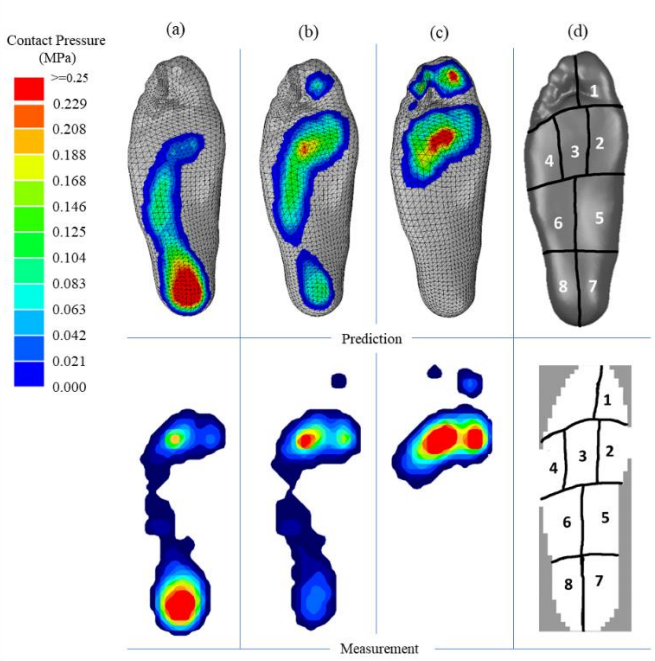

Figure 7. Comparison of foot pressure distribution between model predictions and measurements (a) the first VGRF peak, (b) VGRF valley, and (c) the second VGRF peak, and (d) eight plantar regions

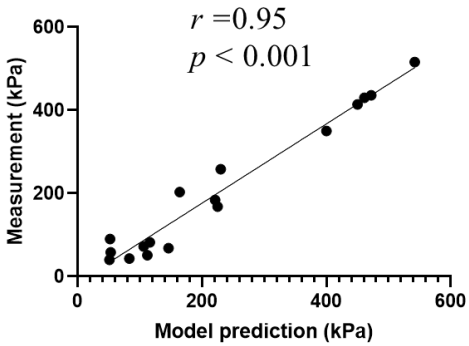

Figure 8. Validation of predicated foot pressure with the experimental measurement using correlation analysis

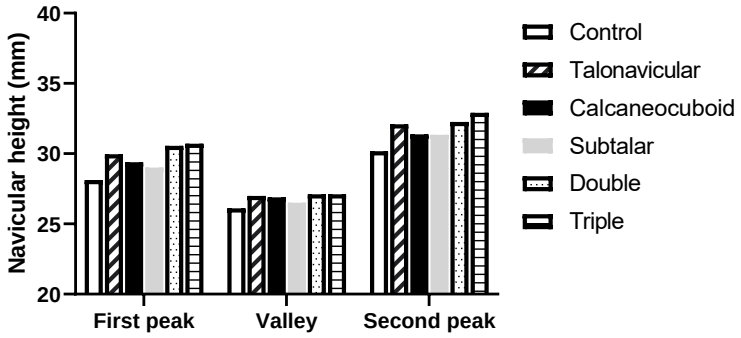

Figure 9. Navicular heights of control and five mid/hindfoot arthrodeses in the first and second peak VGRF as well as the VGRF valley.

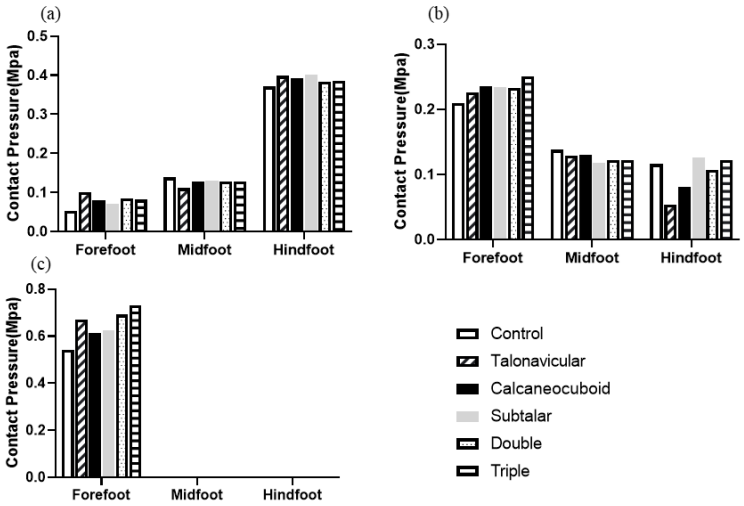

Figure 10. Comparison of peak foot plantar pressure of forefoot, midfoot, and hindfoot among the control and five mid/hindfoot arthrodeses in the (a) first VGRF peak, (b) VGRF valley, and (c) second VGRF peak.

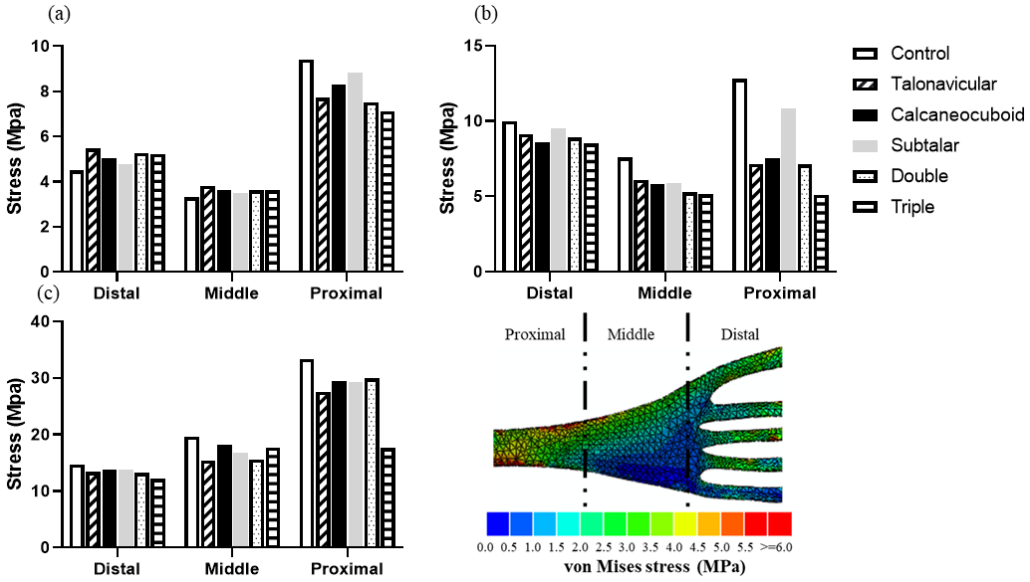

Figure 11. Comparison of peak plantar fascia for the control and five mid/hindfoot arthrodeses conditions in the (a) first VGRF peak, (b) VGRF valley, and (c) second VGRF peak. The regions tied to the foot bones were excluded from the contour. The remaining part of the fascia was divided equally into three parts, including proximal, middle, and distal parts.

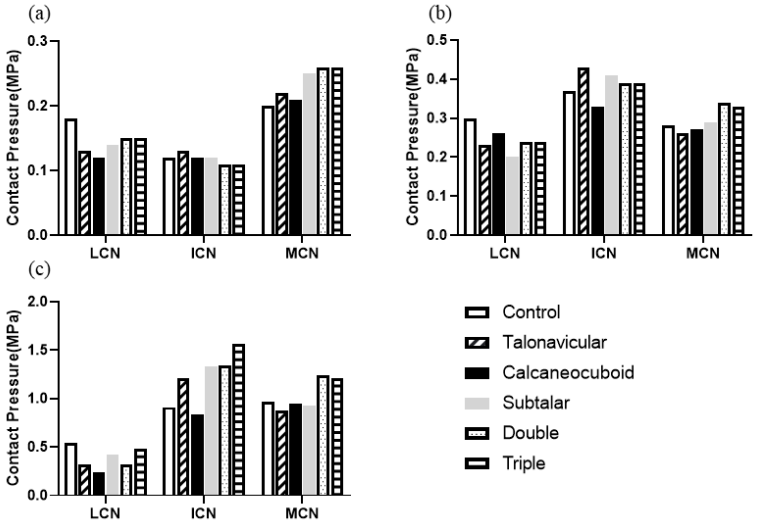

Figure 12. Comparison of peak contact pressures in three joints for the control and five mid/hindfoot arthrodeses conditions in the (a) first VGRF peak, (b) VGRF valley, and (c) second VGRF peak. LCN represents lateral cuneo-navicular, ICN represents intermediate cuneo-navicular, and MCN represents medial cuneo-navicular.

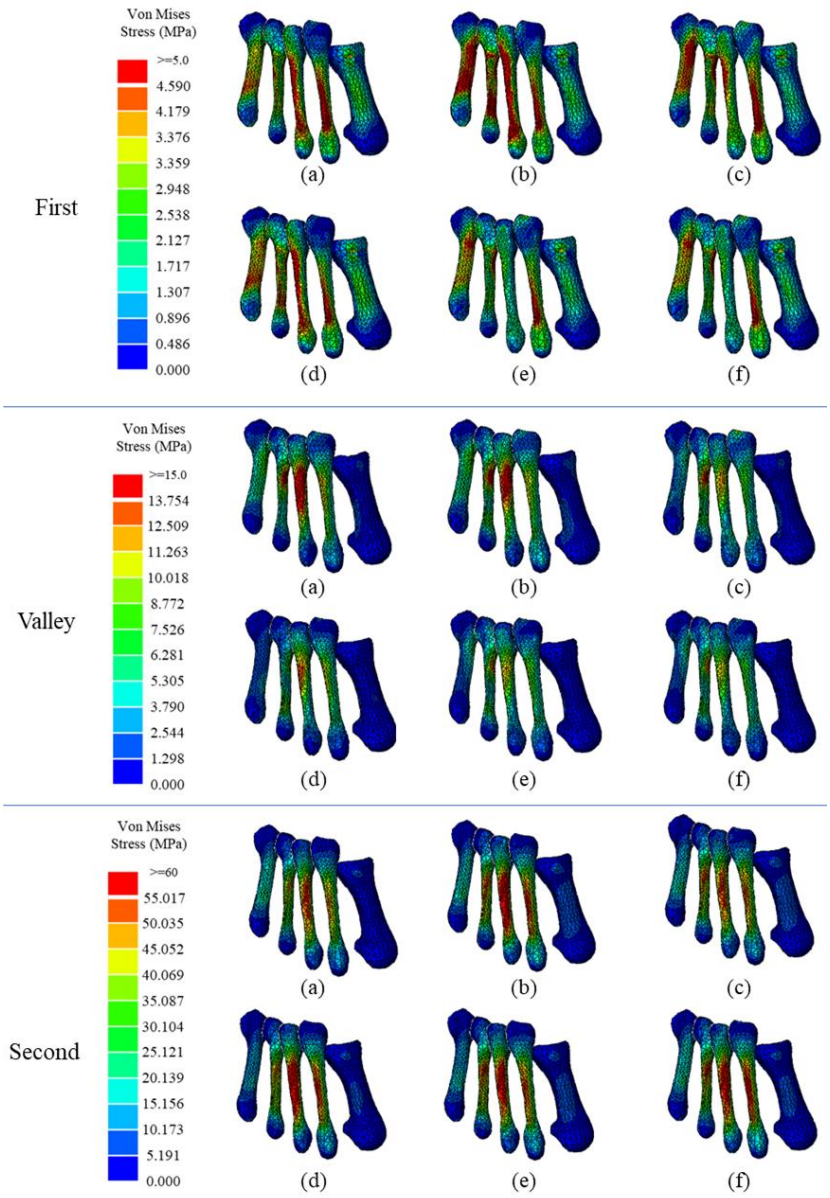

Figure 13. Comparison of peak von Mises stress of five metatarsal bones during first VGRF peak, VGRF valley, and the second VGRF peak for the control and five mid/hindfoot arthrodeses conditions, including (a) control condition, (b) talonavicular arthrodesis, (c) calcaneocuboid arthrodesis, (d) subtalar arthrodesis, (e) double arthrodesis, and (f) triple arthrodesis.

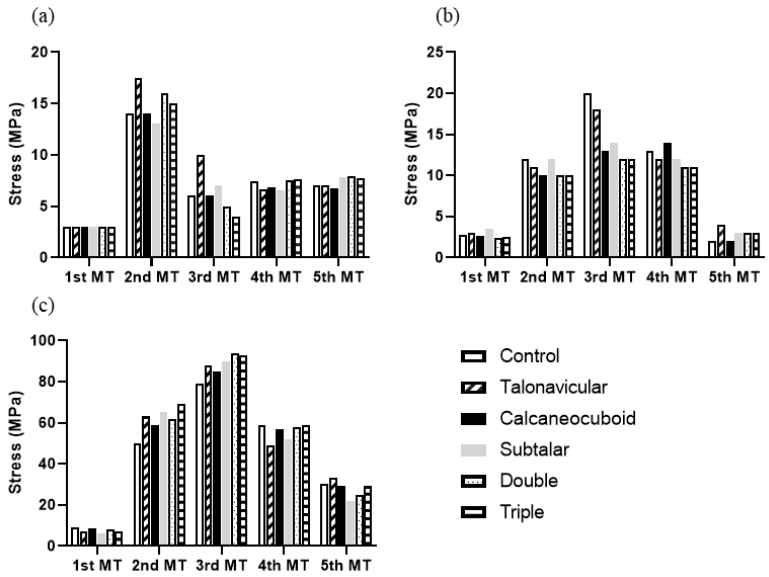

Figure 14. Comparison of peak von Mises stress of five metatarsal bones for the control and five mid/hindfoot arthrodeses conditions in the (a) first VGRF peak, (b) VGRF valley, and (c) second VGRF peak.

Table 1. Material properties of the components in the finite element model

	Elastic modulus (MPa)	Poisson ratio	Cross-section (mm^2)	Element type	Mesh count	References
Skin	1st-order Ogden hyperelastic model (μ= 0.122 MPa, α=18, Thickness: 2.0 mm)		-	Three-node triangular membrane elements (M3D3)	7303	[46]
Bulk soft tissue	second-order polynomial strain hyperelastic model (C_{10}=0.8556, C_{01}=-0.05841, C_{20}=0.03900, C_{11}=-0.02319, C_{02}=0.00851, D_1=3.65273)		-	Linear tetrahedral element (C3D4)	115,468	[47]
Bone	10000	0.34	-	Linear tetrahedral element (C3D4)	104,075	[48]
Ligaments	260	0.4	18.4	Two-node linear three-dimensional elements (T3D2)	200	[49]
Three-dimensional Plantar fascia	350	0.45	-	Linear tetrahedral element (C3D4)	8882	[50]
Ground plate	17000	0.3	-	Linear hexahedra element (C3D8)	19,060	[16]